Journal of Structural Geology, Vol. 14, No. 6, pp. 713 to 721, 1992
Printed in Great Britain

0191-8141/92 $05.00+0.00

Drape folding of compressible elastic layers—I. Analytical solutions for vertical uplift

WILLIAM C. HANEBERG

New Mexico Bureau of Mines and Mineral Resources, New Mexico Insititute of Mining and Technology, Socorro, NM 87801, U.S.A.

(*Received* 12 *March* 1991; *accepted in revised form* 27 *January* 1992)

Abstract—Two new analytical solutions allow the effects of layer thickness, vertical fault zone width and throw, layer compressibility, and basal slip on drape fold geometry to be investigated. Welded (Case I) and non-welded (Case II) lower contacts with step vertical displacement functions and an upper free surface are used as boundary conditions. Comparison of fold profiles, displacement fields and principal stress trajectory fields suggests that fold form yields relatively little information about lower boundary geometry or stress conditions. Drape folds with non-welded contacts, however, are distinctly asymmetric along their lower boundaries. Displacement and principal stress trajectory fields, on the other hand, can be used to distinguish which of the two boundary conditions was used to produce a given theoretical fold. Values of maximum shear stress are much higher along welded contacts than along non-welded contacts, suggesting that faulting and brecciation should be more prevalent along welded contacts. These findings are consistent with published field observations, and suggest that some attributes of theoretical folds—for example, lower boundary geometry and minor fracture orientation—may be used to infer the conditions under which real drape folds were formed

INTRODUCTION

THE bending of layered rocks in response to movement along underlying faults, commonly referred to as drape folding or forced folding, has long been of interest to structural geologists. This paper presents two analytical solutions for displacements and stresses in a compressible elastic layer draped over a vertical fault zone of variable width, building upon earlier work by authors such as Sanford (1959) and Reches & Johnson (1978). These solutions are used to perform a series of numerical experiments in which the effects of layer thickness, fault zone width and lower boundary slip are examined. Although the work described in this paper was begun in an attempt to better understand the origin of large fissures in unconsolidated basin-fill sediments draped over buried faults in Arizona (Carpenter 1989), Nevada (Bell *et al.* 1989, Bell & Hoffard 1990), New Mexico (Haneberg *et al.* 1991) and Texas (Baumgardner & Akhter 1991, Keaton & Shlemon 1991), the results should be of interest to many structural geologists, mining engineers, and mineral or petroleum exploration geologists. A subsequent paper will develop a semi-analytical matrix solution for two-layer drape folds, allowing the influence of lower boundary conditions on structural style to be examined in more detail.

Examples of drape fold geometry can be found in the text by Price & Cosgrove (1990, pp. 247–249) and in the volume edited by Mathews (1978). Laboratory experiments by Sanford (1959), Friedman *et al.* (1976), Logan *et al.* (1978), Whittaker & Reddish (1989) and Withjack *et al.* (1990) illustrate how small-scale drape folds can be formed under controlled conditions. Stearns (1978) discussed in some detail the difference between welded and non-welded contacts between crystalline basement and sedimentary cover, comparing drape fold morphology and regional stratigraphic changes between southern and northern Wyoming. In cases where the lowermost sedimentary layer is a non-ductile sandstone or carbonate, for example the Palisades monocline in Arizona (Reches 1978), the fold is centered over the basement fault and the lower boundary has sinusoidal symmetry (Fig. 1a). In cases where the lowermost sedimentary layer is a ductile shale or evaporite, as in the Rattlesnake Mountain drape fold (Stearns 1978), the fold is believed to be centered above the down-thrown block and the lower boundary is asymmetric (Fig. 1b). According to Stearns, this difference occurs because ductile shales can flow to eliminate any empty space directly above the fault, whereas more brittle sandstones must conform to basement geometry by bending, breaking, or both.

Some geologists, not recognizing the possibility of ductile flow in lower layers, project surface exposures downward using constant layer thickness and infer the presence of either blind thrusts or basement folds in order to construct balanced cross-sections. For example, Anderson (1989) discounts the possibility of basement folding and infers a series of blind thrusts to explain the asymmetry of the Nutria monocline in northwestern New Mexico. Only the Paleozoic and Mesozoic sedimentary cover is exposed at the surface, so the basement structure is speculative. As with most Colorado Plateau monoclines, the upper, possibly overturned, anticlinal hinge has been removed by erosion and only parts of the lower synclinal hinge have been preserved. Therefore, only a little is known about the geometry of the complete monocline, and in particular it is impossible to establish with any certainty whether or not the monocline was originally overturned.

Although thrusting, such as that proposed by Anderson (1989), may be necessary to explain overturned drape fold limbs, the models developed in this paper will

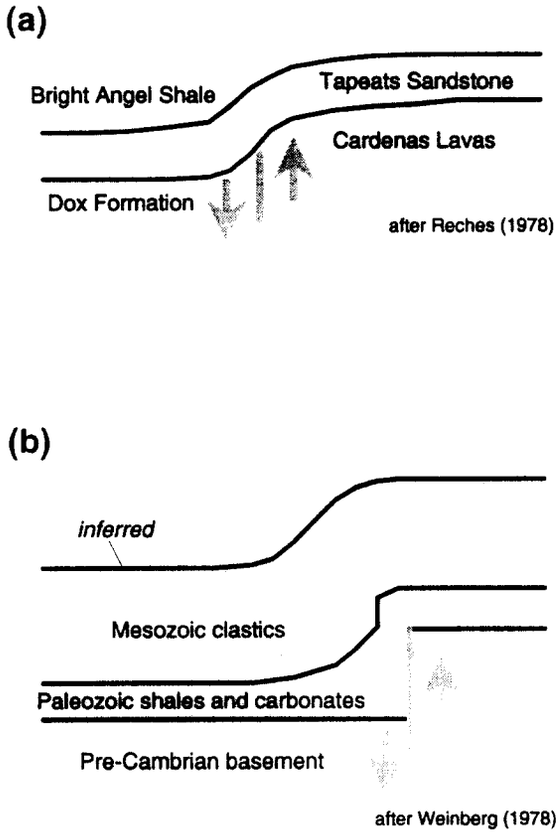

Fig. 1. (a) Schematic cross-section of the lower portion of the Palisades monocline (modified from Reches 1978). Structural relief due to both faulting of the Tapeats Sandstone and regional tilt have been removed to infer drape fold geometry before the Tapeats was disrupted. This is an example of a drape fold with a welded lower contact. (b) Schematic cross-section of the Rattlesnake Mountain drape fold (Stearns 1978), showing the inferred top of the missing Mesozoic section (modified from Weinberg 1978). This is an example of a drape fold with a non-welded lower contact.

show that there is no mechanical reason to require the presence of blind thrusts to account for the asymmetry of non-overturned drape folds. Instead, the asymmetry interpreted as evidence of thrusting by some geologists can be developed solely due to the presence of weak (e.g. shale or evaporite) layers near the base of the drape fold.

Previous analyses

Analytical solutions to both linear elastic and linear viscous problems have been used by other workers to investigate the mechanics of drape folding. The general approach is to assume a state of plane strain, reducing the problem to integration of one or two biharmonic equations. Hafner (1951) used both polynomial and trigonometric solutions to study the effects of various stress boundary conditions, including periodic basal normal and shear stress distributions, on a gravity-loaded layer using polynomial and exponential solutions to the biharmonic equation. Sanford (1959) used trigonometric solutions to analyze the effects of both periodic stress and periodic displacement boundary conditions on a compressible gravity-loaded layer. However, he was able to derive expressions for only six of the eight necessary constants of integration, and had to approximate the remaining two constants by trial and error. Howard (1966) applied Hafner's method to analyze drape folding along the Williams Range Thrust in Colorado. Likewise, Couples (1977) and Couples & Stearns (1978) used trigonometric solutions to combine the effects of square-wave and sawtooth basal normal stress distributions with uniform basal shear stress on an elastic layer, and analyzed stresses in an elastic layer thrusted over an irregular basement. Gangi *et al.* (1977) used a novel solution method, based upon bilateral Laplace transforms, to solve drape fold problems for both welded and free-slipping basal contacts; although mathematically unwieldy, this method allows the effects of non-analytic lower boundary conditions to be examined. Reches & Johnson (1978) investigated the monoclinal flexure of incompressible viscous multilayers by matching stresses and displacements across the boundaries of several single layers and numerically solving for the constants of integration. Koch *et al.* (1981) took a different approach, analyzing the monoclinal flexure of strata over laccoliths in terms of shear stresses and contact strengths in a layered series of thin elastic beams. Most recently, Spencer & Chase (1989) drew upon both polynomial and trigonometric solutions to treat stresses in an elastic layer subject to many different combinations of boundary conditions, including Gaussian normal stress distributions along the upper and lower boundaries.

Although geologists typically envision drape folding as a distinctive process driven by movement along deep seated faults, Reches & Johnson (1978) maintained that folds formed over laccolithic intrusions or basement folds may be indistinguishable from fault-driven drape folding. In other words, the mechanical problem is somewhat divorced from the geological problem. The former is concerned with the response of a layer or layers to some distribution of driving stresses or displacements at depth. The latter, however, is also concerned with the timing and origin of the driving stresses or displacements. Therefore, although references such as Koch *et al.* (1981) and Spencer & Chase (1989) may not seem relevant to the geological problem of drape folding, they are intimately related to the mechanical problem of drape folding.

MECHANICAL MODEL

In this analysis, drape folds are modeled as compressible elastic layers subjected to two combinations of displacement and stress along their lower boundaries, corresponding to Stearns' (1978) welded and non-welded cases. Vertical displacement of $2B_0$ along the lower boundary, akin to movement along a buried vertical fault, is distributed over a horizontal distance of $2h$ (Fig. 2). In both cases, vertical displacement along the lower boundary is specified by a Fourier series approximation of a step with arbitrary height and width.

No horizontal displacement is allowed, meaning that the elastic layer is bonded to the forcing blocks below. In Case II shear stress along the lower boundary is required to vanish, allowing the compressible layer to slip freely over the forcing blocks. This situation might occur if the compressible sedimentary cover were separated from rigid basement rocks by a thin ductile (e.g. shale or evaporite) layer. Normal and shear stresses are required to vanish along the top of the layers in both Case I and Case II, corresponding to the surface of the Earth.

The method of solution employed in this paper has been described in some detail by others; therefore, many intermediate steps are omitted in the interest of brevity. Virtually all of the calculus and algebraic manipulations necessary to obtain the solutions presented here were performed using the computer program "Mathematica" (Wolfram 1988), which also translated results into C language expressions for numerical evaluation.

General solution

This analysis assumes that the drape fold forms in plane strain. General solutions for the two components of displacement, derived following the method of Johnson & Honea (1975) and Reches & Johnson (1978) are, in dimensionless form,

$$\frac{u}{L} = [(c_1 + c_2 z)e^{lz} + (c_3 + c_4 z)e^{-lz}]\frac{l}{n\pi}\cos lx \quad (1)$$

$$\frac{v}{L} = \left\{\left[\frac{(3c_2 - c_1 l) + (\lambda/G)(c_2 - c_1 l)}{n\pi[1 + (\lambda/G)]} - c_2\frac{z}{L}\right]e^{lz} + \left[\frac{(3c_4 + c_3 l) + (\lambda/G)(c_4 + c_3 l)}{n\pi[1 + (\lambda/G)]} + c_4\frac{z}{L}\right]e^{-lz}\right\}\sin lx, \quad (2)$$

where u is horizontal displacement, v is vertical displacement, G and λ are the Lamé constants, and c_1–c_4 are arbitrary constants of integration that will vary according to boundary conditions. The wave number is

$$l = n\pi/L, \quad (3)$$

where L is the wavelength of the drape fold and n is any integer. Layer thickness, which will enter into the particular solutions, is denoted by T. Both (1) and (2) must be solutions to biharmonic equations in u and v (Reches & Johnson 1978), which can be verified by the reader.

The four displacement gradients, found by differentiating (1) and (2), are

$$\frac{\partial u}{\partial x} = -[(c_1 + c_2 z)e^{lz} + (c_3 + c_4 z)e^{-lz}]l\sin lx \quad (4)$$

$$\frac{\partial u}{\partial z} = \{[c_2 + l(c_1 + c_2 z)]e^{lz} + [c_4 - l(c_3 + c_4 z)]e^{-lz}\}\cos lx \quad (5)$$

$$\frac{\partial v}{\partial x} = \left\{\left[\frac{(3c_2 - c_1 l) + (\lambda/G)(c_2 - c_1 l)}{[1 + (\lambda/G)]} - c_2 lz\right]e^{lz} + \left[\frac{(3c_4 + c_3 l) + (\lambda/G)(c_4 + c_3 l)}{[1 + (\lambda/G)]} + c_4 lz\right]e^{-lz}\right\}\cos lx \quad (6)$$

$$\frac{\partial v}{\partial z} = \left\{\left[\frac{(3c_2 - c_1 l) + (\lambda/G)(c_2 - c_1 l)}{[1 + (\lambda/G)]} - c_2(lz + 1)\right]le^{lz} - \left[\frac{(3c_4 + c_3 l) + (\lambda/G)(c_4 + c_3 l)}{[1 + (\lambda/G)]} + c_4(lz - 1)\right]le^{-lz}\right\}\sin lx. \quad (7)$$

Equations (4)–(7) can now be used to determine stresses. For plane strain, the three in-plane components of stress (Malvern 1969, p. 505) are, in this case normalized relative to the shear modulus G,

$$\frac{\sigma_{xx}}{G} = \left(\frac{\lambda}{G} + 2\right)\frac{\partial u}{\partial x} + \frac{\lambda}{G}\frac{\partial v}{\partial z} \quad (8)$$

$$\frac{\sigma_{xx}}{G} = \left(\frac{\lambda}{G} + 2\right)\frac{\partial v}{\partial z} + \frac{\lambda}{G}\frac{\partial u}{\partial x} \quad (9)$$

$$\frac{\sigma_{xz}}{G} = 2\left(\frac{\partial u}{\partial z} + \frac{\partial v}{\partial x}\right). \quad (10)$$

Sign convections used throughout this analysis are illustrated in Fig. 3, and $\sigma_{zx} = \sigma_{xz}$. The weight of the layer, which is neglected throughout this analysis, can be incorporated by the addition of lithostatic terms to the two normal stresses (Hafner 1951). The dimensionless

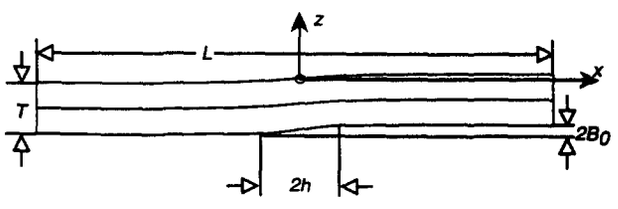

Fig. 2. Illustration of geometric variables used to formulate the mechanical problem. Material properties such as shear modulus and compressibility are discussed in the text and illustrated in Fig. 4.

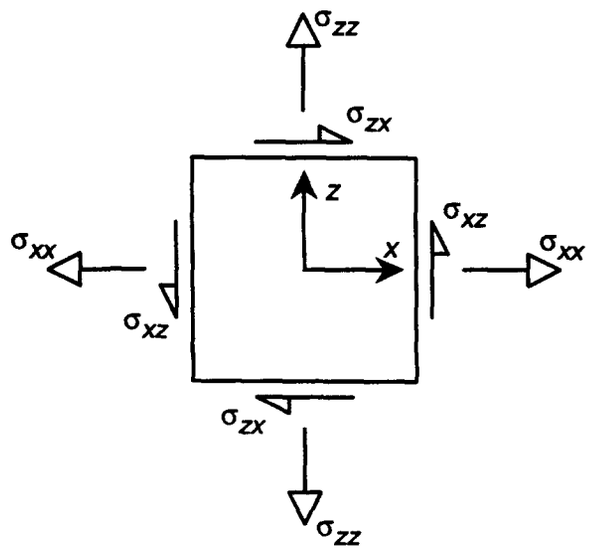

Fig. 3. Sign conventions used in this analysis. Tensile stresses are positive, and equilibrium of moments requires that $\sigma_{xz} = \sigma_{zx}$. Also, note that the z axis is positive-upwards.

material constant λ/G reflects the compressibility of the layer, and is related to Poisson's ratio, ν, by

$$\frac{\lambda}{G} = \frac{2\nu}{1-2\nu}. \tag{11}$$

This compressibility relationship is plotted in Fig. 4.

Particular solutions

Once general solutions for the two components of displacement have been found, solution of the mechanical model requires that two stress or displacement conditions be specified along the upper boundary and two more along the lower boundary (Malvern 1969, p. 499). These boundary conditions are necessary in order to evaluate the four constants of integration c_1–c_4. Throughout this analysis it is assumed that the upper surface of the elastic layer is traction free, representing the surface of the Earth, so that

$$\sigma_{zz} = 0 \tag{12}$$

$$\sigma_{xz} = 0 \tag{13}$$

along $z = 0$. Expressions for σ_{zz} and σ_{xz} are obtained by substituting the displacement gradient equations,(4)–(7), into (8)–(10) as appropriate.

Vertical displacement along the lower boundary, $z = -T$, is given by a Fourier series of the form

$$\frac{v}{L} = \sum_{n=1}^{\infty} b_n \sin lx, \tag{14}$$

where the left-hand side of (14) is given by (2). For the lower boundary geometry used in this paper,

$$b_n = \frac{2B_0/L}{n\pi - 4n^3\pi(h/L)^2}\left[\cos\left(n\pi\frac{h}{L}\right) - \left(\left\{1 - 4n^2\left(\frac{h}{L}\right)^2\left[1 - \cos\left(\frac{\pi}{2}\frac{L}{h}\right)\right]\right\}\cos\left(n\pi\frac{h}{L}\right) - \left[4n^2\left(\frac{h}{L}\right)^2 - 2n\left(\frac{h}{L}\right)\sin\left(n\pi\frac{h}{L}\right)\right]\sin\left(\frac{\pi}{2}\frac{L}{h}\right)\right)(-1)^n\right], \tag{15}$$

which produces a rounded step function geometrically

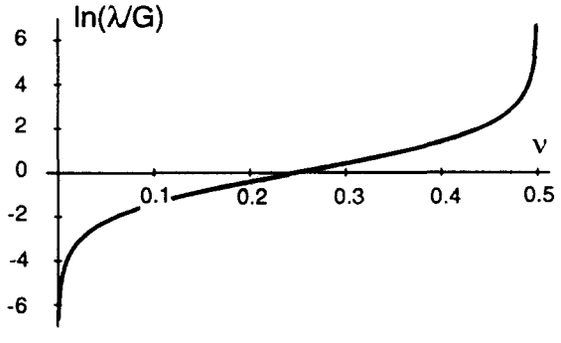

Fig. 4. Relationship of the dimensionless compressibility parameter, λ/G, to Poisson's ratio, ν. The exponential nature of this curve indicates that solutions will be boundless for either perfectly compressible ($\nu = 0$) or perfectly incompressible ($\nu = 0.5$) elastic layers.

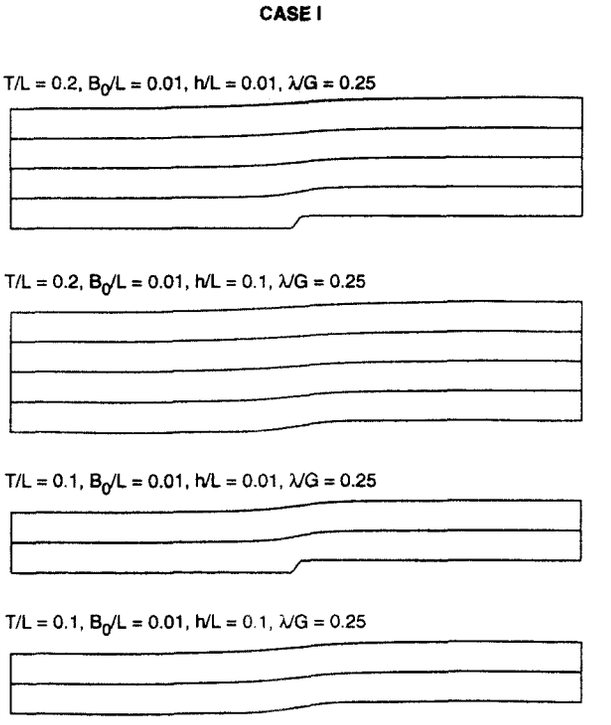

Fig. 5. Forms of some theoretical drape folds with bonded lower contacts (Case I), illustrating the effects of changing layer thickness (T/L) and fault zone width (h/L). All other variables were held constant. The internal markers are all passive and are intended only to help visualize fold geometry.

identical to that used by Reches & Johnson (1978). In general, any Fourier sine series can be used to specify vertical displacement along the lower boundary. One might, for example, derive a more complicated Fourier series to examine deformation over a series of stepped faults.

The fourth boundary condition will be varied in order to investigate the effects of slip along the lower boundary. The two cases to be examined were chosen primarily because (1) they represent the end members in a continuous spectrum of possible cases, and (2) the forms of the boundary condition equations give rise to relatively simple solutions.

Following the example of Reches & Johnson (1978, p. 308), it is assumed that the compressible layer is infinitely long, and that the drape fold represents only one-half wavelength of a periodic fold train. Therefore, it is not necessary to specify boundary conditions at each end of the fold in this case.

Case I: Welded contact. For the first case, the final lower boundary condition is

$$u = 0, \tag{16}$$

where the left-hand side of (16) is given by (1), evaluated at $z = -T$. This corresponds to Stearns' (1978) welded scenario, and is analogous to the problems solved approximately by Sanford (1959) and numerically by Reches & Johnson (1978). The four constants of integration are found by setting $z = 0$ in (12) and (13), and setting $z = -T$ in (15) and (16). This gives rise to a set of four linear equations with four unknowns that, with some effort, can be solved algebraically to yield

$$c_1 = \frac{b_n}{D_1}\left\{e^{3lT}\left[-4 - 2\frac{\lambda}{G} - lT - 2\frac{\lambda}{G}lT - \left(\frac{\lambda}{G}\right)^2 lT\right] + lTe^{lT}\left[1 + 2\frac{\lambda}{G} + \left(\frac{\lambda}{G}\right)^2\right]\right\} \quad (17)$$

$$c_2 = \frac{b_n l}{D_1}(e^{lT} - e^{3lT})\left[1 + 2\frac{\lambda}{G} + \left(\frac{\lambda}{G}\right)^2\right] \quad (18)$$

$$c_3 = \frac{b_n}{D_1}\left\{e^{lt}\left[4 + 2\frac{\lambda}{G} - lT - 2\frac{\lambda}{G}lT - \left(\frac{\lambda}{G}\right)^2 lT\right] + lTe^{3lT}\left[1 + 2\frac{\lambda}{G} + \left(\frac{\lambda}{G}\right)^2\right]\right\} \quad (19)$$

$$c_4 = -c_2, \quad (20)$$

where

$$D_1 = 3 + 4\frac{\lambda}{G} + \left(\frac{\lambda}{G}\right)^2 + e^{2lT}\left[2 - 4\frac{\lambda}{G} - 2\left(\frac{\lambda}{G}\right)^2\right] + e^{4lT}\left[3 + 4\frac{\lambda}{G} + \left(\frac{\lambda}{G}\right)^2\right]. \quad (21)$$

Case II: Non-welded contact. For the second case, free slip is allowed along the bottom of the layer, corresponding to Stearns' (1978) non-welded scenario. Thus, the second lower boundary conditions is

$$\sigma_{xz} = 0. \quad (22)$$

As in Case I, the four constants of integration are found by setting $z = 0$ in (12) and (13), and setting $z = -T$ in (14) and (22),

$$c_1 = -\frac{b_n e^{lT}}{1 + e^{2lT}} \quad (23)$$

$$c_2 = 0 \quad (24)$$

$$c_3 = -c_1 \quad (25)$$

$$c_4 = 0. \quad (26)$$

In either case, final results are found by calculating stresses or displacements for many values of n, in this paper 100, and adding the results together.

RESULTS

The solutions developed above illustrate that drape folding above a vertical fault—even in a single, homogeneous and isotropic elastic layer— is controlled by five factors: (1) layer thickness; (2) fault zone width; (3) fault zone throw; (4) material properties; and (5) the lower boundary conditions. Beyond this, however, the variables of interest will be controlled by the nature of the geologic problem being investigated. For example, if the forms of drape folds are of primary interest, then one might be most interested in comparing geometric details of real and theoretical folds. If the orientation of minor structures associated with drape folds is paramount, then one might be most interested in comparing calculated principal stress trajectories and magnitudes with observed faults, joints and minor folds. Finally, if one is most concerned with the nucleation and growth of small faults, then quantities such as maximum shear stress may be useful tools.

It would be difficult, as well as tedious, to evaluate all possible combinations for the five controlling factors. However, it is possible to systematically evaluate the role of each factor by conducting a series of numerical experiments, which are described below.

The theoretical drape folds in Figs. 6 and 7 illustrate differences in form due to changing layer thickness and fault zone width. Values of $T/L = 0.20$ vs $T/L = 0.10$ and $h/L = 0.01$ vs $h/L = 0.10$ were selected arbitrarily, but the compressibility of $\lambda/G = 0.25$ was chosen as a value typical of sedimentary rocks. Except for the upper and lower boundaries, all of the layering is passive. In other words, the internal markers deform with the elastic layer but have no mechanical effect. They serve only to emphasize fold geometry. The small amount of variation in fold form that does exist is localized along the lower boundaries, and, given only the shape of the upper surface, it would probably be impossible to predict either the fault zone width or the lower boundary condition. Upon first inspection, the slopes of the upper surface of the $h/L = 0.01$ folds may appear to be slightly steeper than the slopes of the $h/L = 0.10$ folds. Close comparison reveals the apparent difference to be an optical illusion.

The asymmetric lower boundary characteristic of Case II folds, for which there is a simple geometric explanation, may seem peculiar. Recall that only two

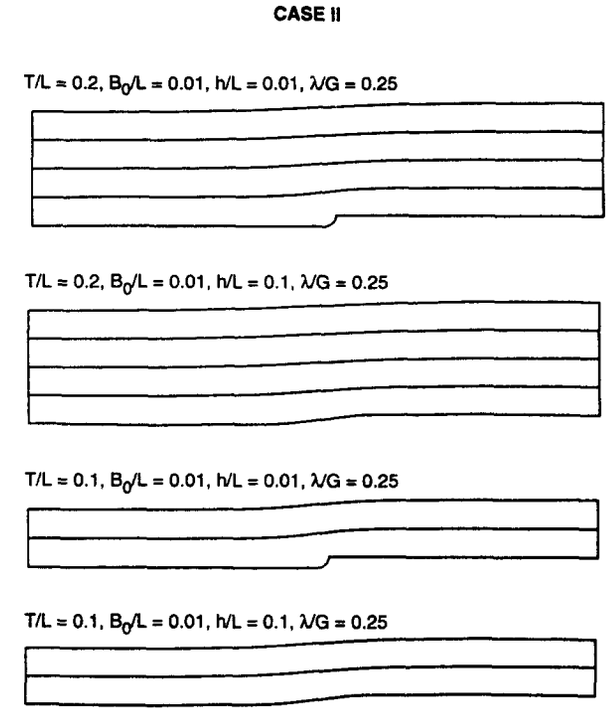

Fig. 6. Forms of some theoretical drape folds with free slip along the lower contact (Case II), illustrating the effects of changing layer thickness (T/L) and fault zone width (h/L). All other variables were held constant. The internal markers are all passive and are intended only to help visualize fold geometry.

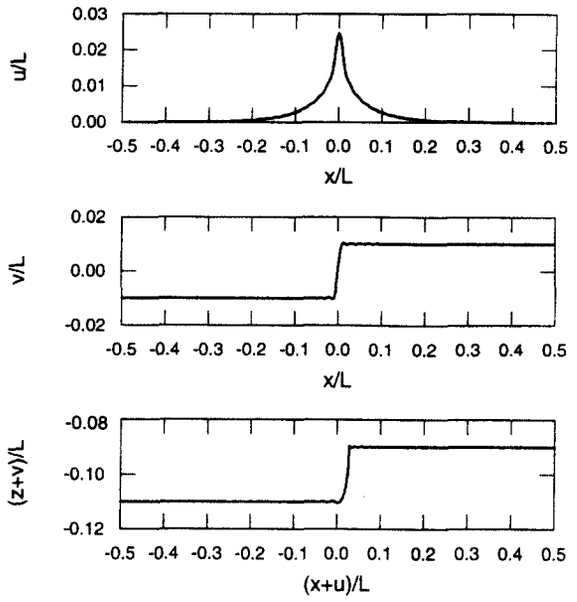

Fig. 7. Plots illustrating components of the asymmetric Case II lower boundary. Geometric and material properties are $T/L = 0.10$, $B_0/L = 0.01$, $h/L = 0.01$, and $\lambda/G = 0.25$. Combination of the cosinusoidally symmetric u component with the sinusoidally symmetric v component results in the asymmetric lower boundary characteristic of Case II folds.

boundary conditions can be specified along the base of the compressible layer. For Case II folds, the lower boundary conditions are of the forms $v/L = \Sigma_{n=1}^{\infty} b_n \sin lx$ and $\sigma_{xz} = 0$. Therefore, the horizontal component of displacement will be non-zero along the lower boundary and, from inspection of (1), will vary with $\cos lx$. When the two non-zero components of displacement are combined to find the deformed co-ordinates of the lower boundary, $(x + u, z + v)$, asymmetry across the fault will result (Fig. 8). This is especially obvious for small values of h/L, because the non-zero horizontal displacement is concentrated over a short distance. Horizontal displacement along the lower boundary is allowable because the model consists of a single, isolated layer along which boundary stresses and displacements are applied. In reality, horizontal displacement would be

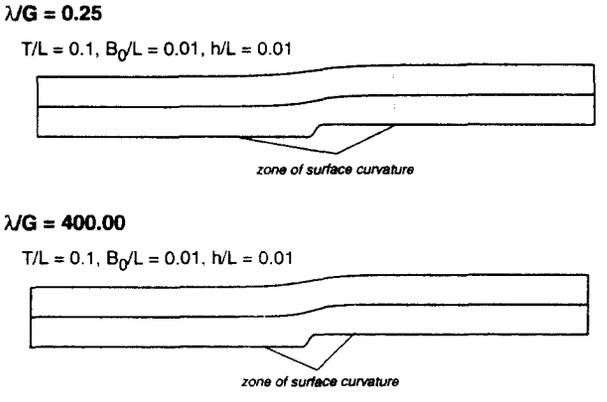

Fig. 8. Effects of changing compressibility on the forms of otherwise identical folded layers subjected to Case I lower boundary conditions. The compressibility parameter $\lambda/G = 0.25$ is equivalent to a Poisson's ratio of $\nu = 0.10$, and the compressibility parameter $\lambda/G = 400$ is equivalent to a Poisson's ratio of $\nu = 0.49$.

constrained by the basement rocks. This point is addressed in more detail in Part II, where the no-shear lower boundary condition is replaced by an easily sheared layer of finite thickness. Under these conditions, asymmetric folding does occur within the easily sheared basal layer, but is not as obvious because it is distributed over a layer of finite, rather than infinitesimal, thickness. In Case I folds, however, the lower boundary conditions are of the forms $v/L = \Sigma_{n=1}^{\infty} b_n \sin lx$ and $u = 0$. Because only one of the lower boundary displacement components is non-zero, Case I folds will retain the symmetry of the non-zero component.

Layer compressibility can also have a minor influence on fold geometry, as illustrated in Fig. 9. The upper fold was formed from a fairly compressible layer, with $\lambda/G = 0.25$, whereas the lower fold was formed from a virtually incompressible layer, with $\lambda/G = 400$. In terms of the more familiar Poisson's ratio, these values are equivalent to $\nu = 0.10$ and $\nu = 0.49$, which is as large a range as one might expect for soil or rock. All other things being equal, the effect of reducing layer compressibility is to increase the tightness of the fold. This difference is most simply expressed in terms of the width of the zone in which the upper boundary of the fold is noticeably curved. The widths of these zones, denoted by vertical gray lines in Fig. 9, are different for the two folds which otherwise differ only in compressibility. If the compressibility contrast is smaller, then the change in fold shape becomes insignificant.

Displacement fields are markedly different for each of the two cases (Fig. 10). In a thin, fairly compressible layer, horizontal displacement directly above the fault zone decreases with depth in Case I but increases exponentially with depth in Case II. The Case II displacement field also serves to emphasize the significance of lower boundary horizontal displacements, which are not allowed in Case I drape folds, on deformed lower boundary shape.

Principal stress orientations for the same two folded layers (Fig. 11) are also noticeably different for Case I and Case II folds. Because tensile stresses are considered positive in this paper, σ_1 is the most tensile or least compressive principal stress and, for the same reason, σ_3 is the least tensile or most compressive principal stress. The requirement of zero horizontal displacement along the lower boundary in Case I drape folds causes principal stress trajectories near the base of the compressible layer to rotate. In contrast, the compressible layer can slip freely over the driving blocks in Case II folds, and principal stress trajectories remain horizontal and vertical along the shear-free lower boundary. Even above the boundary, Case I stress trajectories are broadly curved whereas Case II stress trajectories are generally horizontal and vertical. The only place where Case II stress trajectories are rotated is directly above the fault zone. Even directly above the fault, however, the Case II stress trajectories remain nearly parallel and perpendicular to the layer boundaries.

The overall intensity of stresses developed due to

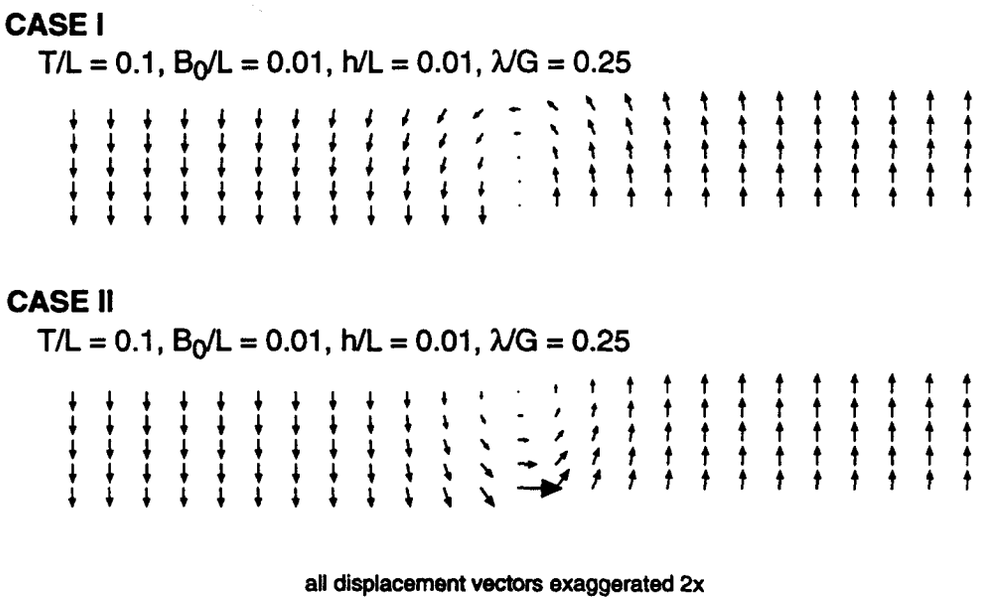

Fig. 9. Resultant displacement vector ($\sqrt{u^2 + v^2}$) fields for thin Case I and Case II folds, with dimensionless parameters as indicated. Arrow length is proportional to displacement magnitude, with horizontal and vertical exaggeration of ×2.

draping is reflected by the maximum shear stress, which is defined as (e.g. Pollard & Segall 1987)

$$\tau_{max} = \tfrac{1}{2}\sqrt{(\sigma_{zz} - \sigma_{xx})^2 + 4\sigma_{xz}^2}. \quad (27)$$

Gray-scale contour plots of maximum shear stress for the Figs. 10 and 11 drape folds are shown in Fig. 12. The largest shear stresses are concentrated near the step in both cases. In Case I the largest values occur directly above the step, whereas in Case II they occur on either side of the step. The mechanical difference between Case I and Case II boundaries is also reflected by the magnitudes of maximum shear stresses for each case. The largest value calculated for the Case I fold is nearly four times the shear modulus, whereas the largest value calculated for the Case II fold is somewhat less than the shear modulus.

DISCUSSION

The forms of the theoretical folds presented in this paper are similar to those described in field studies (e.g. Reches 1978, Stearns 1978) as well as those calculated in previous theoretical studies (e.g. Sanford 1959, Reches & Johnson 1978). Most of the deformation is concentrated very near the buried fault, and both passive marker curvature and stresses decrease towards the upper surface. Most importantly, the forms of theoretical folds produced using Case I and Case II boundary conditions appear similar to real folds in which welded and non-welded lower boundaries have been inferred.

The model results have other implications for field studies in structural geology. For example, Withjack *et al.* (1990), on the basis of clay model experiments,

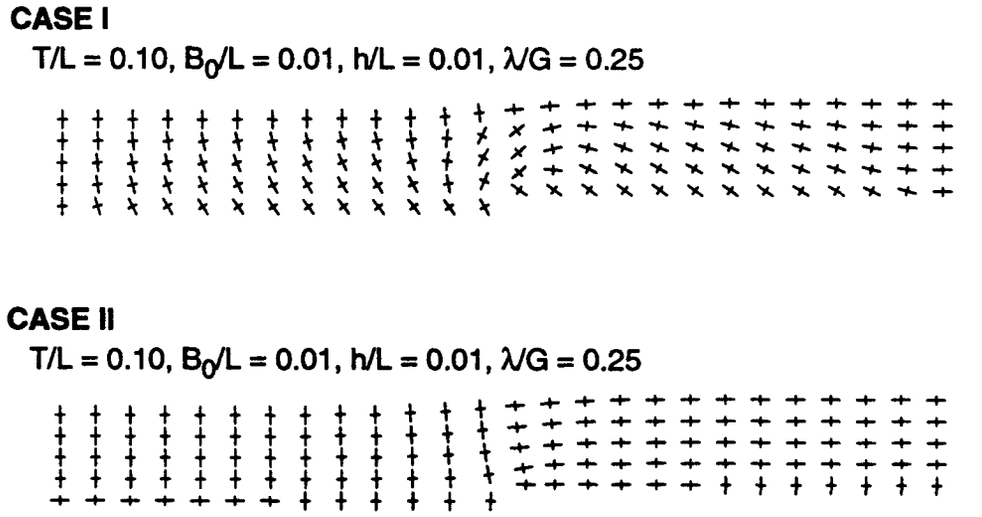

Fig. 10. Principal stress trajectories for folds shown in Fig. 9. The most tensile (or least compressive) principal stress, σ_1, is denoted by the longer axes, whereas the least tensile (or most compressive) principal stress, σ_3, is denoted by the shorter axes.

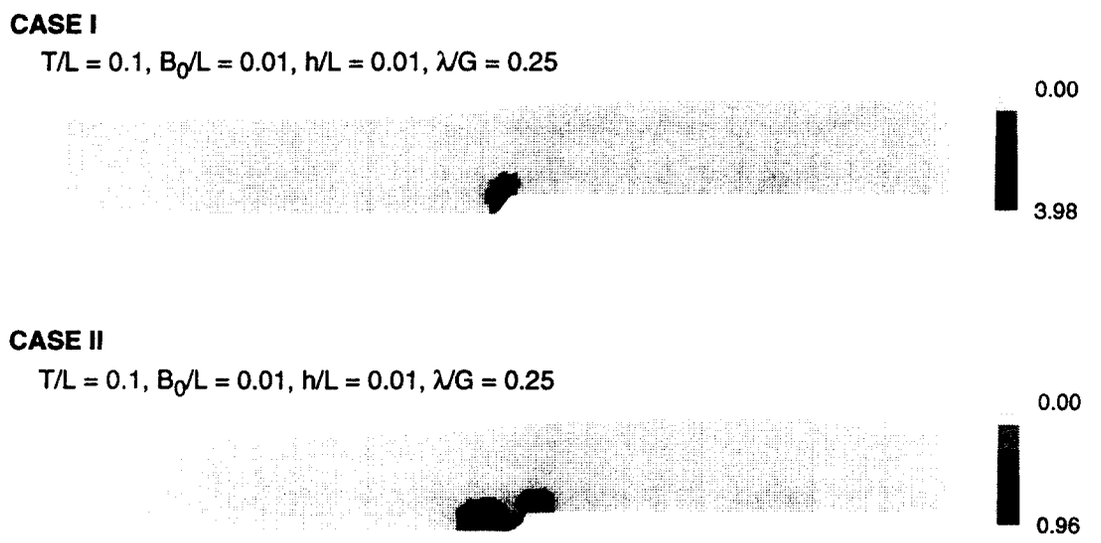

Fig. 11. Maximum shear stress plots for folds shown in Figs. 9 and 10. All values are normalized relative to the shear modulus, G, of the draped layer. Lighter values indicate low levels of shear stress, whereas darker values indicate high levels of shear stress.

suggested that the dip of a buried fault could be inferred from the form of the upper surface of a fold. This is not always true. Comparison of the folds in Figs. 6 and 7 shows that changing fault zone geometry alone has no significant effect on the forms of drape folds. However, the theoretical folds in Fig. 9 show that layer compressibility *does* have an effect on the geometry of folds draped over identical faults. Even though the faults beneath both folds in Fig. 9 are vertical, the conclusions of Withjack *et al.* (1990) would lead one to incorrectly infer that the fault beneath the lower fold is steeper than the fault beneath the upper fold. It is not certain how horizontal extension, which was incorporated into the laboratory models, would affect these results.

A second implication for field studies is that the mechanical stratigraphy of drape-folded sequences must be considered when constructing cross-sections. This is especially true when surface data are projected to depth. If weak strata such as shales or evaporites are present along the bottom of a drape-folded sequence, then it may not be necessary to infer the presence of blind faults to explain asymmetric folds (e.g. Anderson 1989). This finding is consistent with Stearns' (1978) field observations.

Displacement fields in folds subjected to different lower boundary conditions are different, and could provide a tool to discriminate between Case I and Case II lower boundary conditions. Unfortunately, it is impossible to document displacement fields in the ancient folds studied by most structural geologists. Studies of near-surface deformation associated with modern-day groundwater withdrawal (Carpenter 1989), volcanic activity (Wallman *et al.* 1990) or aseismic fault creep (Bell *et al.* 1989, Bell & Hoffard 1990), however, may provide opportunities for the observation of displacement fields in active drape folds. To this end, the author is currently engaged in a project to monitor near-surface deformation due to seasonal groundwater pumping cycles in southern New Mexico. It is believed that cyclic changes in pore water pressure across buried faults in unconsolidated basin-fill deposits cause draping of overlying layers, leading to the development of large earth fissures (Haneberg *et al.* 1991).

Case I stress trajectories are similar to the principal strain trajectories published by Reches & Johnson (1978), who obtained a numerical solution for an incompressible viscous multilayer. The author is not aware of any published examples analogous to the Case II results presented in this paper. Principal stress trajectory fields suggest that ancient Case I and Case II folds might be differentiated on the basis of minor faults and joints within the main structure. For example, joints or mode I cracks propagate parallel to the most compressive principal stress axis (short axes in Fig. 11) and perpendicular to the most tensile principal stress axis (long axes in Fig 11) in order to maximize fracture propagation energy (Pollard & Aydin 1988). Therefore, the existence of broadly curving stress trajectories suggests that joints might exhibit a wide range of dips in Case I drape folds, but only a limited range of dips in Case II drape folds. In both cases, however, joints should be horizontal or subhorizontal above the downthrown basement block and vertical to sub-vertical above the up-thrown block. The orientation of minor faults, which geologists have long assumed to form at angles of about $\pm 30°$ to the most compressive principal stress direction (e.g. Hafner 1951, Couples 1977), might likewise be valuable diagnostic tools.

Finally, the maximum shear stress values calculated for Case I and Case II folds show that much higher shear stresses develop along welded contacts than along nonwelded contacts. The geologic implication is that brecciation should be more prevalent along the base of Case I folds, as suggested by Stearns (1978).

Acknowledgements—This work was supported by the New Mexico Bureau of Mines & Mineral Resources. Allan Sanford provided a reprint of his 1959 paper and read a draft of the manuscript. Discussion with Orin Anderson raised several issues concerning the structural interpretation of some Colorado Plateau monoclines. Comments by Joe Bridwell, Peter Hudleston, Marshall Reiter and two anonymous reviewers helped to improve the clarity of this paper.

REFERENCES

Anderson, O. J. 1989. Basement fault models for the Nutria Monocline. In: *Southeastern Colorado Plateau* (edited by Anderson, O. J., Lucas, S. G., Love, D. W. & Cather S. M.). New Mexico Geological Society 40th Annual Field Conference Guidebook, 28 September–1 October 1989, 60–61.

Baumgardner, R. W., Jr & Akhter, M. S. 1991. Geomorphology and surface-water hydrology of part of the Hueco Basin, West Texas. *West Texas geol. Soc. Bull.* **30**, 5–27.

Bell, J. W., Ramelli, A. R., DePolo, C. M., Maurer, D. K. & Prudic, D. E. 1989. Extensional cracking along an active normal fault: A case for creep on a Basin and Range fault? (Abs.). *Seism. Res. Lett.* **60**, 30.

Bell, J. W. & Hoffard, J. L. 1990. Late Quaternary tectonic setting for a possible fault creep event in the Pine Nut Mountains area, western Nevada. *Geol. Soc. Am. Abs. w. Prog.* **22**, 7.

Carpenter, M. C. 1989. Earth-fissure movements associated with fluctuations in ground-water level, south-central Arizona, 1980–84 (Abs.). *Proc. 28th Int. Geol. Congr, Volume I*, Washington, DC, 243.

Couples, G. 1977. Stress and shear fracture (fault) patterns resulting from a suite of complicated boundary conditions with application to the Wind River Mountains. *Pure & Appl. Geophys.* **115**, 113–133.

Couples, G. & Stearns, D. W. 1978. Analytical solutions applied to structures of the Rocky Mountain foreland on local and regional scales. In: *Laramide Folding Associated with Basement Block Faulting in the Western United States* (edited by Matthews, V., III). *Mem. geol. Soc. Am.* **151**, 313–336.

Friedman, M., Handin, J., Logan, J. M., Min, K. D. & Stearns, D. W. 1976. Experimental folding of rocks under confining pressure: Part III—Faulted drape folds in multi-lithologic layered specimens. *Bull. geol. Soc. Am.* **87**, 1049–1066.

Gangi, A. F., Min, K. D. & Logan, J. M. 1977. Experimental folding of rocks under confining pressure: Part IV—Theoretical analysis of faulted drape folds. *Tectonophysics* **42**, 227–260.

Hafner, W. 1951. Stress distributions and faulting. *Bull. geol. Soc. Am.* **62**, 373–398.

Haneberg, W. C., Reynolds, C. B. & Reynolds, I. B. 1991. Geophysical characterization of soil deformation associated with earth fissures near San Marcial and Deming, New Mexico. In: *Land Subsidence* (edited by Johnson, A. I.) (*Proc. 4th Int. Symp. on Land Subsidence*, Houston, Texas). *Int. Ass. Hydrol. Sci. Publ.* **200**, 271–280.

Howard, J. H. 1966. Structural development of the Williams Range Thrust, Colorado. *Bull. geol. Soc. Am.* **77**, 1247–1264.

Johnson, A. M. & Honea, E. 1975. A theory of concentric, kink, and sinusoidal folding and of monoclinal flexuring of compressible, elastic multilayers, III. Transition from sinusoidal to concentric-like to chevron folds. *Tectonophysics* **27**. 1–38.

Keaton, J. R. & Shlemon, R. J. 1991. The Fort Hancock earth fissure system, Hudspeth County, Texas: uncertainties and implications, In: *Land Subsidence* (edited by Johnson, A. I.) (*Proc. 4th Int. Symp. on Land Subsidence*, Houston, Texas). *Int. Ass. Hydrol. Sci. Publ.* **200**, 281–290.

Koch, F. G., Johnson, A. M. & Pollard, D. D. 1981. Monoclinal bending of strata over laccolithic intrusions. *Tectonophysics* **74**, T21–T31.

Logan, J. M., Friedman, M. & Stearns, M. T. 1978. Experimental folding of rocks under confining pressure: Part VI—Further studies of faulted drape folds. In: *Laramide Folding Associated with Basement Block Faulting in the Western United States* (edited by Matthews, V., III). *Mem. geol. Soc. Am.* **151**, 79–100.

Malvern, L. E. 1969. *Introduction to the Mechanics of a Continuous Medium*. Prentice-Hall, Englewood Cliffs, New Jersey.

Matthews, V. III (editor). 1978. *Laramide Folding Associated with Basement Block Faulting in the Western United States. Mem. geol. Soc. Am.* **151**.

Pollard, D. D. & Aydin, A. 1988. Progress in understanding jointing over the past century. *Bull. geol. Soc. Am.* **100**, 1181–1204.

Pollard, D. D & Segall, P. 1978. Theoretical displacements and stresses near fractures in rock: with applications to faults, joints, veins, dikes, and solution surfaces. In: *Fracture Mechanics of Rock* (edited by Atkinson, B. K.). Academic Press, London, 277–349.

Price, N. J. & Cosgrove, J. W. 1990. *Analysis of Geological Structures*. Cambridge University Press, Cambridge.

Reches, Z. 1978. Development of monoclines: Part I. Structure of the Palisades Creek branch of the East Kaibab monocline, Grand Canyon, Arizona. In: *Laramide Folding Associated with Basement Block Faulting in the Western United States* (edited by Matthews, V., III). *Mem. geol. Soc. Am.* **151**, 235–272.

Reches, Z. & Johnson, A. M. 1978. Development of monoclines: Part II. Theoretical analysis of monoclines. In: *Laramide Folding Associated with Basement Block Faulting in the Western United States* (edited by Matthews, V., III). *Mem. geol. Soc. Am.* **151**, 273–312.

Sanford, A. R. 1959. Analytical and experimental study of simple geologic structures. *Bull geol. Soc. Am.* **70**, 19–52.

Spencer, J. E. & Chase, C. G. 1989. Role of crustal flexure in initiation of low-angle normal faults and implications for structural evolution of the Basin and Range Province. *J. geophys. Res.* **94**, 1765–1775.

Stearns. D. W. 1978. Faulting and forced folding in the Rocky Mountains foreland. In: *Laramide Folding Associated with Basement Block Faulting in the Western United States* (edited by Matthews, V., III). *Mem. geol. Soc. Am.* **151**, 1–37.

Wallman, P. C., Pollard, D. D., Hildreth, W. & Eichelberger, J. C. 1990. New Structural limits on magma chamber locations at the Valley of Ten Thousand Smokes, Katmai National Park, Alaska. *Geology* **18**, 1240–1243.

Weinberg, D. M. 1978. Some two-dimensional kinematic analyses of the drape-fold concept. In: *Laramide Folding Associated with Basement Block Faulting in the Western United States* (edited by Matthews, V., III). *Mem. geol. Soc. Am.* **151**, 51–78.

Whittaker, B. N. & Reddish, D. J. 1989. *Subsidence: Occurrence, Prediction, and Control*. Amsterdam, Elsevier.

Withjack, M. O., Olson, J. & Peterson, E. 1990. Experimental models of extensional forced folds. *Bull. Am. Ass. Petrol. Geol.* **74**, 1038–1054.

Wolfram, S. 1988. *Mathematica: A System for Doing Mathematics by Computer*. Addison-Wesley, Redwood City, California.